

Role of codeposited impurities during growth. II. Dependence of morphology on binding and barrier energies

Rajesh Sathiyarayanan,^{1,2,*} Ajmi BH. Hamouda,^{1,3,†} A. Pimpinelli,^{1,4,‡} and T. L. Einstein^{1,§}

¹*Department of Physics, University of Maryland, College Park, Maryland 20742-4111, USA*

²*Department of Chemical Engineering, The Pennsylvania State University, University Park, Pennsylvania 16802, USA*

³*Physics Department, Sciences Faculty of University of Monastir, 5019 Monastir, Tunisia*

⁴*Scientific Attaché, French Embassy in the United States, Consulate General of France, Houston, Texas 77056, USA*

(Received 31 July 2010; revised manuscript received 20 October 2010; published 24 January 2011)

In an accompanying article we showed that surface morphologies obtained through codeposition of a small quantity (2%) of impurities with Cu during growth (step-flow mode, $\theta = 40$ ML) significantly depends on the lateral nearest-neighbor binding energy (E_{NN}) to Cu adatom and the diffusion barrier (E_d) of the impurity atom on Cu(0 0 1). Based on these two energy parameters, E_{NN} and E_d , we classify impurity atoms into four sets. We study island nucleation and growth in the presence of codeposited impurities from different sets in the submonolayer ($\theta \leq 0.7$ ML) regime. Similar to growth in the step-flow mode, we find different nucleation and growth behavior for impurities from different sets. We characterize these differences through variations of the number of islands (N_i) and the average island size with coverage (θ). Further, we compute the critical nucleus size (i) for all of these cases from the distribution of capture-zone areas using the generalized Wigner distribution.

DOI: 10.1103/PhysRevB.83.035424

PACS number(s): 68.55.Ln, 68.35.Dv, 81.15.Aa, 05.40.—a

I. INTRODUCTION

Small quantities of impurities can significantly alter surface morphologies obtained in epitaxial growth.¹ In an accompanying article,² hereafter referred to as I, we showed that midtransition metallic impurities can account for growth instabilities observed on Cu vicinals.^{3–5} In addition, we showed that, depending on their NN binding energy to Cu atoms (E_{NN}) and their terrace diffusion barrier (E_d), codeposition of these impurity atoms result in different surface morphologies. Even though a thorough understanding of the role of impurities in epitaxial growth of metals is not available at present, it is clear that impurities could play an important role in nanostructuring vicinal surfaces. In this article, we discuss in detail the classification of impurities into sets briefly mentioned in I.² We also show that differences in growth behavior for impurities from different sets are present in the submonolayer growth regime.

As mentioned briefly in I, impurity atoms can be classified into four sets based on their E_{NN} and E_d values (cf. Fig. 1; the details of calculating the values of E_{NN} and E_d are discussed in I). The sets are named using the chemical symbols of the elements in the set and the sequence of the elements in the set name is determined by their E_{NN} value. All the vapor-phase impurity atoms, O, C, and S, form the first set, henceforth called set OCS. All of these atoms, despite adsorbing strongly on Cu(0 0 1), actually repel Cu adatoms at nearest-neighbor positions ($E_{NN} < 0$). The repulsion is strongest in the case of O. The second set consists of the elements Ag, Sn, Zn, and Al. The E_{NN} (with the exception of Al) and E_d values of all the atoms in the AgSnZnAl set are smaller than the corresponding values for Cu. The electronic configuration of all elements in this set consists of either a completely filled d orbital (Ag, Sn, Zn) or a no valence d orbital (Al). The E_{NN} values of elements in the PdNiSi set are close to the E_{NN} value of Cu but their diffusion barriers are higher than (1.2–1.5 times) that of Cu. Except for Si, the other elements in this set have nearly filled d orbitals. The last set of impurities consists of the midtransition

elements Co, Fe, Mn, and W, hence called set CoFeMnW. Both their E_{NN} (1.2–1.8 times) and E_d (~ 1.6 times) values are higher than the corresponding values of Cu.

Using kinetic Monte Carlo (KMC) simulations on a solid-on-solid model, we study island nucleation and growth behavior in the submonolayer regime for the cases of pure Cu and Cu codeposited with 2% impurity atoms. We characterize the island nucleation and growth behavior using certain key quantities, such as number of islands (N_i), average island size (AIS), and distribution of capture-zone (CZ) areas. Section II gives the details of our KMC simulations and computation of N_i , AIS, and the CZ-area distribution (CZD). Our results and discussions are presented in Sec. III. Section IV deals with the computation of the critical nucleus size (i) for all of these cases.

II. COMPUTATIONAL DETAILS

We used a two-species solid-on-solid (SOS) model and the underlying lattice was taken to be simple cubic. A detailed description of our model and the relevant energy parameters can be found in I. We used a 800×800 (in units of lattice sites) lattice and atoms were deposited on the surface at $F = 0.05$ ML/s till a coverage (θ) of 0.7 ML was reached; we took temperature $T = 425$ K. While computing the number of islands (N_i), we treat isolated atoms (monomers) as single-atom islands. The AIS is the areal spread of the island at the first layer measured in units of lattice sites. In all of our simulations, some limited nucleation in the second layer occurs only for PdNiSi and CoFeMnW impurities, with further instances of nucleation in the third layer very rare. Hence AIS provides an excellent measure of the number of atoms in islands. We used IDL[®] (Interactive Data Language) to construct CZs around the centers of mass of islands. For the computation of the centers of mass, the heights of the islands were taken to be 1 ML. Isolated atoms were treated as single-atom islands during the construction of CZs.⁶

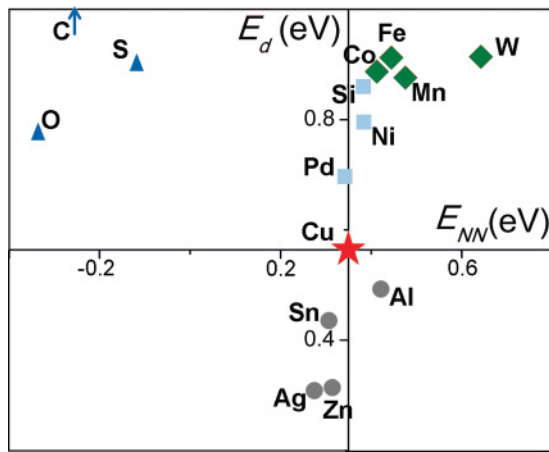


FIG. 1. (Color online) Plot of E_{NN} and E_d values for candidate impurity atoms (except C, whose values lie beyond the range of this plot) relative to the values for Cu (origin). Each set is marked with a distinct symbol: blue triangles, OCS impurities; gray disks, AgSnZnAl impurities; cyan squares, PdNiSi impurities; and green diamonds, CoFeMnW impurities.

III. NUCLEATION AND GROWTH IN THE PRESENCE OF THE VARIOUS IMPURITIES

In the submonolayer regime, deposition of pure Cu results in the formation of monatomic height islands. Figure 2(a) shows the surface at 0.3 ML coverage. For the case of pure Cu, nucleation in the second layer is very rare for $\theta \leq 0.7$ ML. This behavior is consistent with the smooth layer-by-layer growth observed in the step-flow mode for Cu. At the temperature used in our simulations ($T = 425$ K), Cu atoms diffuse freely on the surface and combine with already nucleated islands. The number of islands (N_i) shows little

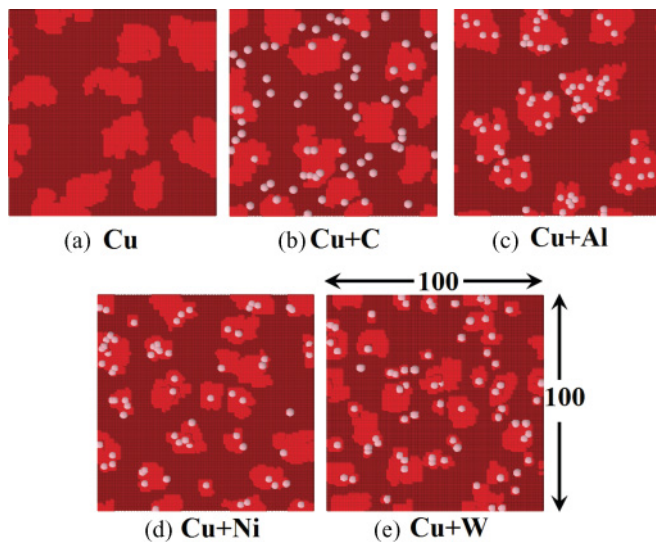


FIG. 2. (Color online) Surface morphologies after a deposition of 0.3 ML of (a) pure Cu and Cu codeposited with 2% of (b) C, (c) Al, (d) Ni, and (e) W impurities. The darker (brown) atoms denote substrate atoms, the lighter (bright red) atoms denote Cu adatoms, and the pale (whitish-gray) atoms on the adatom layer are the impurities. The lateral dimensions of the panels are 100×100 in units of lattice spacings (1 lattice spacing = 2.57 \AA).

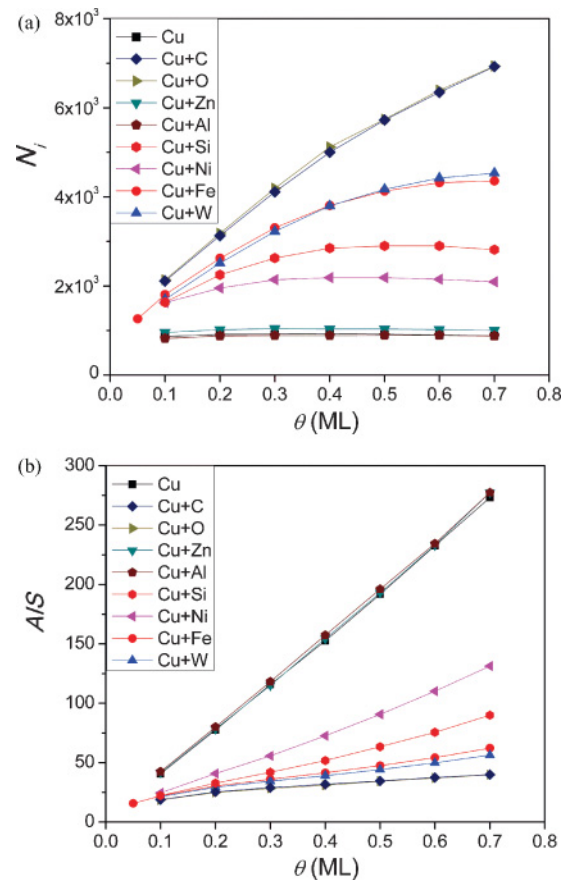


FIG. 3. (Color online) Dependence of (a) number of islands (N_i) and (b) AIS on coverage (θ). The computations were done on a 1000×1000 grid of sites.

variation with θ [cf. Fig. 3(a)], whereas the AIS increases linearly with θ [cf. Fig. 3(b)]. For $\theta > 0.4$ ML, N_i decreases with θ , indicating the onset of coalescence of islands. This phenomenology is consistent with the standard picture of MBE epitaxial growth.⁷ For all the impurities in our study, the AIS tends to increase linearly with θ as well, at least up to large θ .

Since the barriers for impurities in the AgSnZnAl are smaller than the corresponding barriers for Cu, codepositing 2% of Zn or Al impurities with Cu also leads to qualitatively similar results. Similar to the case of pure Cu, nucleation in the second layer is very rare for Cu codeposited with AgSnZnAl impurities [see Fig. 2(c)]. Also, the variation of N_i with θ in the presence of these two impurities is very similar to the behavior observed for pure Cu. For all coverages, the AIS obtained with the codeposition of either Zn or Al impurities is very close to the value obtained for pure Cu [cf. Fig. 3(b)]. Figure 2(c) shows that Al atoms are located in the interior of Cu islands.

In the case of C and O impurities, N_i increases rapidly with θ throughout the regime. Since O and C repel Cu atoms at NN positions, they separate from Cu islands. Both impurities have very high barriers for terrace diffusion; hence, they remain immobile at the simulation temperature. As a result, the surface consists of two types of adatom structures: (i) large Cu islands with very few O or C atoms in them and

(ii) single O or C atoms [see Fig. 2(b)]. For all coverages, single-atom islands form a huge proportion (approximately 60–88%) of the total number of islands. Further, the proportion of single-atom islands increases with θ . When Ni or Si atoms (impurities from the PdNiSi set) are codeposited with Cu, N_i increases linearly with θ for small coverages ($\theta \leq 0.3$ ML) and remains almost constant for $0.4 \leq \theta \leq 0.5$ ML. Beyond a certain coverage ($\theta = 0.5$ for Ni, 0.6 for Si), coalescence sets in, resulting in a decrease in N_i with θ . Figure 2(d) shows that the islands are smaller compared to the case of pure Cu with correspondingly smaller AIS values than pure Cu [see Fig. 3(a)]. Figure 2(d) also shows that Ni impurities are found inside the islands.

Island nucleation behavior in the submonolayer regime is very similar for the cases of Fe and W impurities. The N_i and AIS values for both Fe and W impurities are close to each other for all coverages (see Fig. 3). For both cases, N_i increases with coverage (θ) but the rate of increase becomes smaller with coverage (θ). For neither impurity does coalescence of islands occur. As is clear from Fig. 2(e), many small islands (≤ 10 atoms) form on the surface during the codeposition of W impurities. Such small islands also form for Fe impurities, as reflected in the much smaller (compared to pure Cu) AIS values. The proportion of small islands (≤ 10 atoms) to the total number of islands is 26–35% for Cu with W impurities and 24–38% for Cu with Fe impurities but it is only 2–11% for pure Cu (but the number of monomer impurities is very small). The proportion monotonically decreases with increasing θ for all of these cases, and the lower end of the values occur at $\theta = 0.7$ ML. Furthermore, as θ increases, N_i approaches a constant while the AIS continues to rise, indicating that small islands coalesce into larger ones. This behavior is consistent with results for multilayer growth.² All of these small islands contain an impurity atom, which once again shows that impurities act as nucleation centers for the formation of islands.

Some limited nucleation occurs in the second layer in the cases of PdNiSi and CoFeMnW set impurities, while extremely rare instances of third-layer nucleation occurs only for CoFeMnW impurities at high coverages ($\theta \geq 0.5$ ML). Neglecting the case of OCS impurities, in which the presence of single-atom islands clouds the picture, our results show that higher E_{NN} values between Cu and impurity atoms leads to higher N_i values at all coverages [cf. Fig. 3(a)], consistent with the results in Ref. [8]. Our KMC simulations have shown that distinct island nucleation behavior is obtained depending on the type of impurity codeposited with Cu. In addition to that, the panels in Fig. 3 show that similar behavior (exemplified by overlapping curves) occurs when Cu is codeposited with two different impurities from the same set, justifying our characterization of impurities into sets. To further quantify the differences in island nucleation behavior, we have also computed the distribution of capture-zone areas. The following section discusses these distributions.

IV. DISTRIBUTION OF CAPTURE-ZONE AREAS: THE GENERALIZED-WIGNER DISTRIBUTION

An important parameter in characterizing submonolayer epitaxial growth is the critical-nucleus size (i), i.e., the size

of the largest unstable island on that surface. The value of i depends on quantities like the bond strength, temperature, and deposition flux (F). Studies based on simulations have shown that the island-size distribution (ISD) satisfies a scaling relation in island size over total deposition⁹ and is uniquely determined by i .¹⁰ This connection led to several attempts at finding an analytic expression for describing ISDs,^{10–13} though none were very simple. A simple description for ISDs has remained elusive due to the following reasons: (i) the mean-field nature of the approach that neglects spatial fluctuations in island sizes and (ii) the dependence of ISD on the ratio of the monomer diffusion coefficient (D) to that of the deposition flux (F). To overcome these difficulties, Mulheran and Blackman¹⁴ proposed an alternative approach to extract i from the CZD. However, due to the complexity involved in extracting i in this approach, a semiempirical formula was normally used to extract i from experimental data.

Random matrix theory has been very successful in handling fluctuations in energy-level spacings,¹⁵ and the Wigner surmise^{16,17} [cf. Eq. (1)] derived using random matrix ideas gives an excellent description of spacing distributions in a wide range of physical systems,^{15,18}

$$P_\beta(s) = a_\beta s^\beta e^{-b_\beta s^2}, \quad b_\beta = \left[\frac{\Gamma(\frac{\beta+2}{2})}{\Gamma(\frac{\beta+1}{2})} \right]^2, \quad a_\beta = \frac{2b_\beta^{(\beta+1)/2}}{\Gamma(\frac{\beta+1}{2})}, \quad (1)$$

where s is the size of the capture zone divided by its mean value. The constants b_β and a_β are fixed by this unit-mean condition and normalization, respectively. In these problems, β takes on the values 1, 2, or 4, depending on the symmetry of the problem.

In the field of surface science, the Wigner distribution was generalized to describe the terrace-width distributions of steps¹⁹; in this approach the exponent β takes on arbitrary values (typically between 2 and 10) that are simply related to a dimensionless form of the strength of the step-step repulsion. Recently, Pimpinelli and Einstein¹⁸ showed that the fluctuations in the CZ areas are similar to the fluctuations in terrace widths on vicinal surfaces and that the generalized Wigner distribution (GWD) gives an excellent description of CZD during island growth. In two dimensions (2D) their mean-field analysis suggested that the fit parameter $\beta = i + 1$. Improved simulations^{20,21} compared to those¹⁴ cited in Ref. 18 show that $\beta = i + 2^-$ better accounts for the extensive new numerical data. An analysis going beyond mean field corroborates this result.²² The GWD gives an excellent fit for the CZD for data from both simulations¹⁸ and experiments involving growth of pentacene with pentacenequinone impurities.^{23,24} The GWD has just been applied to a variety of different systems, including Ge/Si(001) nanoislands,²⁵ parasexyphenyl islands on SiO₂,²⁶ and C₆₀ on ultrathin SiO₂.²⁷ At the same time, the single-parameter gamma distribution $G_\alpha(s) = [\alpha^\alpha / \Gamma(\alpha)] s^{\alpha-1} e^{-\alpha s}$ gives a comparably good description of the CZD.

In 1D, the spacing distribution of N interacting particles is determined by the range of interparticle interaction up to nearest-neighbors results in the single-parameter gamma distribution $[G_\alpha(s)]$, whereas an infinite-range interaction results in GWD.²⁸ Since it is hard to identify the range of interaction in the case of CZs, no formal justification can be

made for the choice of fitting function. While limited and noisy data often make it difficult to select the correct fitting function based on fitting quality, the GWD fit is preferable due to the simple connection between the fit parameter β and the critical-nucleus size i . We know of no comparable way to extract directly physical information about the system from the fit parameter α of $G_\alpha(s)$. [However, one can extract i by using that observation that for $\alpha \approx 2\beta + 1$, $G_\alpha(s)$ and $P_\beta(s)$ are similar over the region where both are sizable,^{22,27} so $\alpha \approx 2i + 3$.] We also emphasize that even if there is some uncertainty in the offset needed to go from i to β , the GWD approach clearly shows changes to i when impurities are added, as seen in the decrease of β by 2 in island nucleation experiments when pentacenequinone impurities are codeposited with pentacene.²³

Even though derivations and numerical tests of the GWD treated the deposition of a single species, the procedure gave useful insights regarding the nucleation of pentacene islands with pentacenequinone impurities.²³ Also, the GWD gives a very good fit²⁴ for the CZD of InAs quantum dots on GaAs.²⁹ In extending the GWD-based approach to two-species deposition there is ambiguity in the definition of i . For impurities on Cu, this issue is especially important for the OCS and the CoFeMnW impurity sets, whose E_d values are much higher than that of Cu atoms. Due to very high diffusion barriers, codeposition of these impurities leads to the formation of either single-atom (in the case of OCS impurities) or few-atom (CoFeMnW set impurities) islands on the surface along with large islands. Additionally, the GWD formalism strictly applies only during the early stages of nucleation, before the onset of coalescence. In spite of these issues, our results show that the GWD gives a very good fit to our data (cf. Fig. 4). The fits are good even for coverages beyond the onset of coalescence of islands. To determine the fit exponent β , we used the nonlinear fitting function in MATHEMATICA, and all the data points were weighted equally. The β values obtained

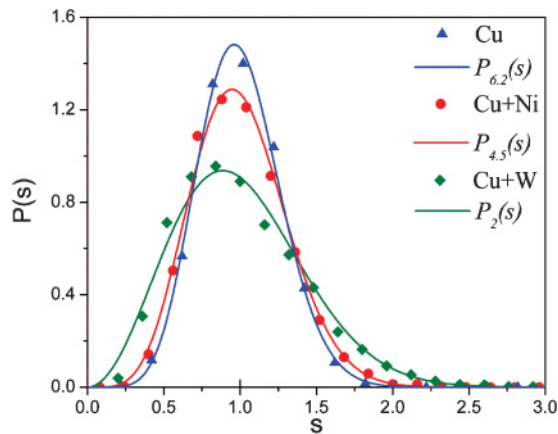


FIG. 4. (Color online) Distribution of CZ areas (CZD) from our simulations (symbols) fitted with the GWD (solid curves): pure Cu at $\theta = 0.6$ ML (blue triangles) fitted with $P_{6,2}(s)$ (blue curve), Cu with 2% Ni impurities at $\theta = 0.4$ ML (red circles) fitted with $P_{4,5}(s)$ (red curve), and Cu with 2% W impurities at $\theta = 0.2$ ML (green diamonds) fitted with $P_2(s)$ (green curve). The case of pure Cu at $\theta = 0.6$ ML falls in the coalescence regime.

TABLE I. The values of β obtained from the GW fits to our simulation data. In each case (except pure Cu), the impurity concentration is 2%. Impurities are grouped by their sets, in order of decreasing β . The values in bold font correspond to the island coalescence regime. For Cu + Fe, $\beta = 2.3$ for $\theta = 0.05$.

θ (ML) \rightarrow	0.1	0.2	0.3	0.4	0.5	0.6	0.7
Cu	4.5	4.4	4.7	5.3	6.0	6.2	6.0
Cu + Al	5.2	5.3	5.8	6.0	6.2	6.3	7.0
Cu + Zn	4.5	5.7	5.6	6.5	6.7	7.2	7.1
Cu + Ni	2.9	3.5	3.8	4.5	4.9	5.5	5.9
Cu + Si	2.5	2.7	3.3	3.5	4.0	4.3	4.9
Cu + W	2.2	2.0	2.3	2.6	2.7	2.8	2.9
Cu + Fe	2.1	2.2	2.4	2.9	3.1	3.3	3.5
Cu + C	1.9	1.7	1.6	1.7	1.5	1.4	1.4
Cu + O	1.9	1.6	1.7	1.4	1.3	1.2	1.1

from our fits are listed in Table I. The variation of β with coverage θ is plotted in Fig. 5.

Several interesting results emerge from the GWD fits to our simulation data (cf. Table I). For pure Cu, β remains a constant during the initial stages of nucleation. Recent simulations scrutinizing the CZD for two models of point islands²⁰ and earlier work on compact islands^{9,13} report no noteworthy dependence on θ in the pre-coalescence regimes. Except for the case of OCS impurities, β increases monotonically with θ . The tendency for β to rise with θ (i.e., for the distribution to narrow) in the aggregation regime corresponds to a narrowing of the distribution, consistent with a decrease in the number of adatoms,⁷ and seems a consequence of the more complicated interactions (and consequent correlations) in the cases with impurities. An increase in β was seen in the recent experiments on Ge/Si(001) nanoislands for Ge coverages ranging from 0.2 ML to 2.0 ML²⁵ (as well as in early numerical work characterizing CZs¹⁴). While we have not explored this behavior in any detail, it is plausible that the islands get bigger at higher coverage and so the size of the smallest stable island increases as in ripening.³⁰

Taking $\beta = i + 2^-$ implies that i lies between 2 and 3 for $\theta \leq 0.4$ ML. The fit parameter β continues to increase for θ above 0.4 ML (coalescence regime). Similar trends are

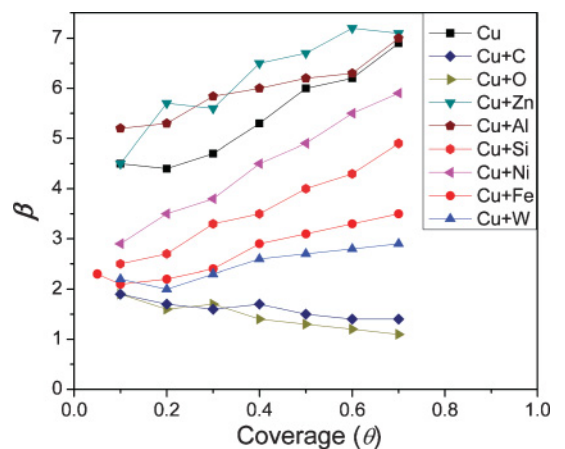


FIG. 5. (Color online) Dependence of β on coverage (θ) when Cu is codeposited with 2% of impurity atoms.

obtained for Zn and Al impurities. For the same coverage, the β values for AgSnZnAl impurities are slightly higher than the corresponding value for pure Cu, which implies an increase in i value during the codeposition of AgSnZnAl impurities. This increase in i can be attributed to the higher mobility (smaller E_d) of AgSnZnAl impurities compared to Cu atoms. The β values for O and C impurities lie between 1 and 2 and β decreases with coverage throughout the regime. Using $\beta = i + 2^-$ leads to negative i values, especially for higher θ values, for O and C impurities. At the same time, we also find that the GWD does not give a good fit to the CZD at higher θ values ($\theta \geq 0.5$ ML) for O and C impurities. Both features suggest a breakdown of the GWD scenario. To understand this behavior recall that E_{NN} is negative (repulsive) for OCS but no other set. Hence, OCS impurities are not likely to spawn islands; they form monomer “islands” as seen in Fig. 2(b). The impurities tend to “poison” much of the surface, so the Cu atoms cluster into a relatively small number of islands which then grow, as graphed in Fig. 3.

For the CoFeMnW set impurities, the obtained β values are much less (by 2–4) than those for pure Cu, indicating a significant reduction in the critical-nucleus size. This reduction in i is understandable because the CoFeMnW impurities have higher barriers for diffusion and, hence, are immobile at the experimental temperature range. Due to stronger bonds with Cu atoms, these impurities act as nucleation centers for the formation of islands, as reflected in the large number of small islands in Fig. 2(e). Hence, similar to the OCS impurities, $i = 0$ for the CoFeMnW impurities. Since they do not separate from Cu islands, unlike OCS impurities, the behavior of β with θ for the CoFeMnW impurities is similar to the cases of Cu with AgSnZnAl, PdNiSi impurities and pure Cu. For all coverages, the β values for PdNiSi impurities lie between the β values for pure Cu and those for Cu with CoFeMnW impurities. The PdNiSi impurities have higher barriers for diffusion than Cu and hence, have a smaller i value than Cu. At the same

time, unlike CoFeMnW impurities, they are not immobile at the simulation temperature, which is also confirmed by the absence of small islands in the case of Ni impurity [cf. Fig. 2(d)].

V. CONCLUSIONS

Using DFT-based VASP calculations and KMC simulations, we have studied the effects of codeposited impurities on growth morphologies in both (i) step-flow mode² and (ii) submonolayer regime. In this study, we have shown that codeposition of a small quantity of impurities leads to very different nucleation and growth behavior in the submonolayer regime. Further, we have shown that impurities can be grouped into sets based on their E_{NN} and E_d values and the resulting growth morphologies, both in the step-flow mode and the submonolayer regime, depend on the particular group the impurity atom belongs to. Since the type of impurity determines the number of islands (N_i), and hence island density, and AIS, this provides a useful method to engineer surface morphologies through the selection of the right type of impurity. The CZD is very well described by the generalized Wigner distribution and the critical nucleus size (i) derived from the generalized Wigner fit provides useful insights into the nucleation and growth behavior in the presence of impurity atoms.

ACKNOWLEDGMENTS

Work at the University of Maryland was supported by NSF-MRSEC, Grant No. DMR 05-20471, with ancillary support from the Center for Nanophysics and Advanced Materials. This research was supported in part by NSF through TeraGrid resources provided by NCSA under Grant No. TG-DMR070003N. We thank Dr. Diego Luis González Cabrera and Dr. Kwangmoo Kim for helpful interactions.

*srjesh@umd.edu; rajessat@in.ibm.com; Current and permanent address: IBM Semiconductor Research and Development Center, Bangalore 560045, India.

†ajmi.hammouda@fsm.rnu.tn

‡On leave from LASMEA, UMR 6602 CNRS/Université Blaise Pascal, Clermont 2, F-63177 Aubière cedex, France.

§einstein@umd.edu

¹A. BH. Hamouda, T. J. Stasevich, A. Pimpinelli, and T. L. Einstein, *J. Phys. Condens. Matter* **21**, 084215 (2009), and references therein.

²A. BH. Hamouda, R. Sathiyarayanan, A. Pimpinelli, and T. L. Einstein, *Phys. Rev. B*, **83**, 035423 (2011).

³T. Maroutian, L. Douillard, and H.-J. Ernst, *Phys. Rev. Lett.* **83**, 4353 (1999).

⁴T. Maroutian, L. Douillard, and H.-J. Ernst, *Phys. Rev. B* **64**, 165401 (2001).

⁵N. Néel, T. Maroutian, L. Douillard, and H.-J. Ernst, *J. Phys. Condens. Matter* **15**, S3227 (2003), and references therein.

⁶For computational ease, we did not apply periodic boundary conditions, used in the KMC runs, during the construction of CZs.

Hence, CZs were not constructed around the islands closest to the lattice boundary. As a result, a small portion of islands (at most 12.6%) were left out during the computation of CZD.

⁷J. G. Amar, F. Family, and P.-M. Lam, *Phys. Rev. B* **50**, 8781 (1994).

⁸M. Kotrla, J. Krug, and P. Šmilauer, *Phys. Rev. B* **62**, 2889 (2000).

⁹M. C. Bartelt and J. W. Evans, *Phys. Rev. B* **46**, 12675 (1992); *Surf. Sci.* **298**, 421 (1993); *J. Vac. Sci. Technol. A* **12**, 1800 (1994).

¹⁰J. G. Amar, F. Family, and P. M. Lam, *Phys. Rev. B* **50**, 8781 (1994); J. G. Amar and F. Family, *Phys. Rev. Lett.* **74**, 2066 (1995).

¹¹J. G. Amar and M. N. Popescu, *Phys. Rev. B* **69**, 033401 (2004); F. Shi, Y. Shim, and J. G. Amar, *ibid.* **71**, 245411 (2005); *Phys. Rev. E* **74**, 021606 (2006).

¹²J. A. Blackman and P. A. Mulheran, *Phys. Rev. B* **54**, 11681 (1996); P. A. Mulheran and D. A. Robbie, *Europhys. Lett.* **49**, 617 (2000); P. A. Mulheran, *ibid.* **65**, 379 (2004).

¹³J. W. Evans, P. A. Thiel, and M. C. Bartelt, *Surf. Sci. Rep.* **61**, 1 (2006).

¹⁴P. A. Mulheran and J. A. Blackman, *Phys. Rev. B* **53**, 10261 (1996).

- ¹⁵M. L. Mehta, *Random Matrices*, 2nd ed. (Academic, New York, 1991).
- ¹⁶F. Haake, *Quantum Signatures of Chaos* (Springer, Berlin, 1991).
- ¹⁷T. Guhr, A. Müller-Groeling, and H. A. Weidenmüller, *Phys. Rep.* **299**, 189 (1998).
- ¹⁸A. Pimpinelli and T. L. Einstein, *Phys. Rev. Lett.* **99**, 226102 (2007), and references therein.
- ¹⁹T. L. Einstein, *Appl. Phys. A* **87**, 375 (2007), and references therein.
- ²⁰F. Shi, Y. Shim, and J. G. Amar, *Phys. Rev. E* **79**, 011602 (2009).
- ²¹M. Li, Y. Han, and J. W. Evans, *Phys. Rev. Lett.* **104**, 149601 (2010).
- ²²A. Pimpinelli and T. L. Einstein, *Phys. Rev. Lett.* **104**, 149602 (2010).
- ²³B. R. Conrad, E. Gomar-Nadal, W. G. Cullen, A. Pimpinelli, T. L. Einstein, and E. D. Williams, *Phys. Rev. B* **77**, 205328 (2007).
- ²⁴T. L. Einstein and A. Pimpinelli, *Bull. Am. Phys. Soc.* **54**, 545 (2008).
- ²⁵S. Miyamoto, O. Moutanabbir, E. E. Haller, and K. M. Itoh, *Phys. Rev. B* **79**, 165415 (2009). They comment that capture zone analysis becomes relevant only once the density of islands is such that the area of a circle having the diffusion length as its radius becomes comparable to the mean area of the capture zones.
- ²⁶S. Lorbek, G. Hlawacek, and C. Teichert, submitted for publication.
- ²⁷M. A. Groce, B. R. Conrad, W. G. Cullen, E. D. Williams, and T. L. Einstein, (unpublished).
- ²⁸D. L. González Cabrera, A. Pimpinelli, and T. L. Einstein, (unpublished).
- ²⁹M. Fanfoni, E. Placidi, F. Arciprete, E. Orsini, F. Patella, and A. Balzarotti, *Phys. Rev. B* **75**, 245312 (2007).
- ³⁰J. B. Hannon, C. Klünker, M. Giesen, H. Ibach, N. C. Bartelt, and J. C. Hamilton, *Phys. Rev. Lett.* **79**, 2506 (1997) shows island ripening on Cu(001), albeit not in the context of growth.